Available online at www.sciencedirect.com
SCIENCE DIRECT
Physics Letters A 355 (2006) 110–117
PHYSICS LETTERS A
www.elsevier.com/locate/pla

Solitary dynamo waves

Joanne Mason [a,*], Edgar Knobloch [b]

[a] *High Altitude Observatory, National Center for Atmospheric Research, Boulder, CO 80307, USA*
[b] *Department of Physics, University of California, Berkeley, CA 94720, USA*

Received 27 July 2005; received in revised form 7 February 2006; accepted 9 February 2006

Available online 17 February 2006

Communicated by A.P. Fordy

Abstract

Long dynamo waves are a characteristic feature of interface dynamo models with spatially localized α and Ω effects. The evolution of such waves is described by the modified Korteweg–de Vries equation. Solutions to this equation take the form of solitary waves, breathers, and snoidal and cnoidal waves, and represent nonlinear waves of magnetic activity that migrate towards the equator, as observed on the Sun. Averaging techniques extend the theory to longer times and relate the amplitude of these waves to the dynamo number.

Keywords: Mean-field dynamo theory; mKdV equation

1. Introduction

Mean-field dynamo theory [8,15] provides a description of the mechanism that is believed to be responsible for the generation of the large-scale magnetic field in stars and planets. The mechanism relies on the generation of toroidal field from a poloidal one via differential rotation (the Ω-effect) together with the regeneration of the poloidal field via the interaction of the small-scale flows and magnetic fields (the α-effect). The saturation of the instability is achieved through the back-reaction of the field on the flow, but in the kinematic regime (in which the flow is prescribed) the mechanism is most often modeled by the suppression of the α-effect. Recently, it has been realized that the instability works more efficiently if the locations of the α and Ω effects are separated in space; such a separation is natural in the solar dynamo if the dynamo is located below the convection zone, in a region known as the solar tachocline [14,16].

Recently, Mason et al. [6] considered a simple analytically tractable model of this process. Both α and Ω are taken to be localized in thin spatially disjoint layers. The dispersion relation describing infinitesimal waves can be obtained analytically, and reveals the presence of two types of waves: long waves whose wavelength is large compared to the vertical extent L of the system, and short waves whose wavelength is comparable to L. The long mode is particularly interesting because its nonlinear evolution obeys at leading order an integrable partial differential equation, the modified Korteweg–de Vries equation [7]. This fact can be traced to the invariance of the dynamo equations under $A \to A + \text{const}$, where A is the (vector) potential for the poloidal magnetic field. This observation in turn suggests the possibility of *solitary* dynamo waves, although the version of the problem studied in Ref. [7] was not general enough to permit such waves.

In this Letter we show that if the model is slightly generalized solitary dynamo waves are indeed possible, and explore their properties. In addition, we describe solutions in the form of cnoidal waves, snoidal waves, kinks and breathers. The results are unexpected since the dynamo equations constitute a (forced) dissipative system, and may be of interest in connection with more realistic models of the dynamo process. In the interest of brevity we omit all details of the calculations; these are similar to those in Ref. [7].

2. The model

We consider an idealized nonlinear mean-field dynamo in which the α and Ω effects are spatially separated. For sim-

* Corresponding author.
E-mail address: jmason@hao.ucar.edu (J. Mason).

0375-9601/$ – see front matter
doi:10.1016/j.physleta.2006.02.013

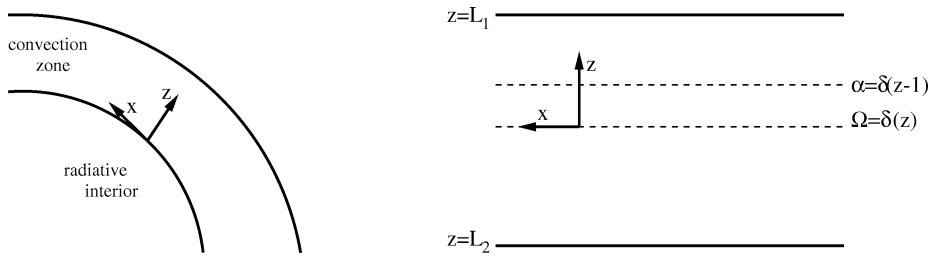

Fig. 1. The geometry of the model. Local Cartesian coordinates are defined on the interface of the convection zone and the tachocline at a point in the northern hemisphere, with x increasing poleward and z with radius ($L_1 > 1$, $L_2 < 0$).

plicity, we take both of these to be spatially localized, with the former situated at $z = 1$ (representing the effect of the convection zone) and the latter located at $z = 0$ (representing the solar tachocline). The magnetic field $\mathbf{B}(x,z,t) \equiv \nabla \times A\mathbf{e}_y + B\mathbf{e}_y$ obeys the dimensionless dynamo equations [4,8]

$$\frac{\partial A}{\partial t} = \alpha(z)B + \nabla^2 A, \tag{2.1}$$

$$\frac{\partial B}{\partial t} = D\Omega(z)\frac{\partial A}{\partial x} + \nabla^2 B, \tag{2.2}$$

where $A(x,z,t)\mathbf{e}_y$ is the vector potential of the poloidal magnetic field, $B(x,z,t)$ is the toroidal field, $\alpha(z) = \delta(z-1)/(1+B^2) \approx \delta(z-1)(1-B^2)$, $\Omega(z) = \delta(z)$ and $D \equiv \alpha_0\Omega_0 z_0^3/\eta_0^2$ is the dynamo number. The form of α represents quenching of the α effect as the field amplifies and provides the sole nonlinearity in the problem. Alternative mechanisms for saturating the dynamo instability are discussed in Ref. [9].

We solve these equations in the semi-infinite domain $-\infty < x < \infty$, $L_2 \leqslant z \leqslant L_1$ for waves that travel in the negative x direction, i.e., towards the equator (Fig. 1). Here $z = L_1 > 1$ represents the top of the convection zone, while $z = L_2 < 0$ lies in the radiative interior below the tachocline, with boundary conditions obtained by matching the magnetic field inside the layer to an external potential field. In a thin layer geometry such a procedure leads to the boundary conditions [13]

$$B(x, z = L_{1,2}, t) = 0, \qquad \frac{\partial A}{\partial z}(x, z = L_{1,2}, t) = 0. \tag{2.3}$$

Thus the toroidal magnetic field is confined in $L_2 < z < L_1$ while the poloidal magnetic field is normal to the layer at $z = L_{1,2}$ at leading order in its aspect ratio. In the following we increase the dynamo number D to trigger the onset of the dynamo instability.

It should be noted that, except at the locations of the α and Ω effects responsible for magnetic field generation, the equations for A and B are diffusion equations. Solutions in the three regions $L_2 < z < 0$, $0 < z < 1$, $1 < z < L_1$ satisfying the boundary conditions at $z = L_1$ and $z = L_2$ are therefore simple to write down. These then have to be matched across $z = 0$ and $z = 1$ subject to the requirement that A and B are continuous and their derivatives satisfy the jump conditions

$$\left[\frac{\partial A}{\partial z}\right]_{z=0} = 0, \qquad \left[\frac{\partial B}{\partial z}\right]_{z=0} + D\frac{\partial A}{\partial x}\bigg|_{z=0} = 0, \tag{2.4}$$

$$\left[\frac{\partial A}{\partial z}\right]_{z=1} + \frac{B}{1+B^2}\bigg|_{z=1} = 0, \qquad \left[\frac{\partial B}{\partial z}\right]_{z=1} = 0, \tag{2.5}$$

obtained by integrating the model equations across $z = 0$ and $z = 1$, respectively.

3. Longwave amplitude equation

Infinitesimal solutions of the form $[A(x,z,t), B(x,z,t)] = [a(z), b(z)]\exp(pt + ikx)$, $p \equiv \sigma + i\omega$, satisfy the dispersion relation, cf. [6],

$$4q^2\sinh^2\big[q(L_1 - L_2)\big] + ikD\sinh\big[2q(L_1 - 1)\big]\sinh[2qL_2] = 0, \tag{3.1}$$

where $q^2 \equiv p + k^2$. Waves with wavenumber $k = \epsilon \ll 1$ traveling towards the equator have frequency $\omega = \epsilon\omega_{10} + \epsilon^3\omega_{30} + \epsilon^5\omega_{50} + \cdots$ and set in at dynamo number $D_c = D_0 + \epsilon^2 D_2 + \epsilon^4 D_4 + \cdots$, where

$$\omega_{10} = \sqrt{\frac{3}{2(2L_1 - 1) - (L_1 + L_2)^2}},$$

$$D_0 = -\frac{\omega_{10}(L_1 - L_2)^2}{L_2(L_1 - 1)}. \tag{3.2}$$

The requirement that $\omega_{10} \in \Re$ places restrictions upon the relative values of L_1 and L_2, as shown in Fig. 2. For fixed L_1, $\ell \equiv -L_2/L_1$ must be within the range $0 \leqslant \ell_{\omega_1} < \ell < \ell_{\omega_2}$, say. For $L_1 = 2$ we have $0 < \ell \lesssim 2.2$. Fig. 3, also computed for $L_1 = 2$, shows D_2 and ω_{30} as functions of ℓ; D_2 vanishes at $\ell_d \approx 1.5$, while ω_{30} vanishes at $\ell \approx 1.3$. Note that $\ell_{\omega_1} \leqslant \ell_d \leqslant \ell_{\omega_2}$. When $D_2 > 0$ ($\ell < \ell_d$) the instability sets in with infinite wavelength, but when $D_2 < 0$ ($\ell > \ell_d$) the onset wavelength is finite, although long.

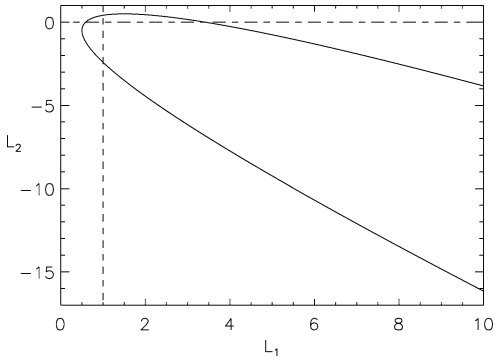

Fig. 2. The region of the (L_1, L_2) plane where the frequency ω_{10} is real. By definition $L_1 > 1$ and $L_2 < 0$ (dashed lines) and the frequency ω_{10} is real inside the subdomain bounded by the solid curve.

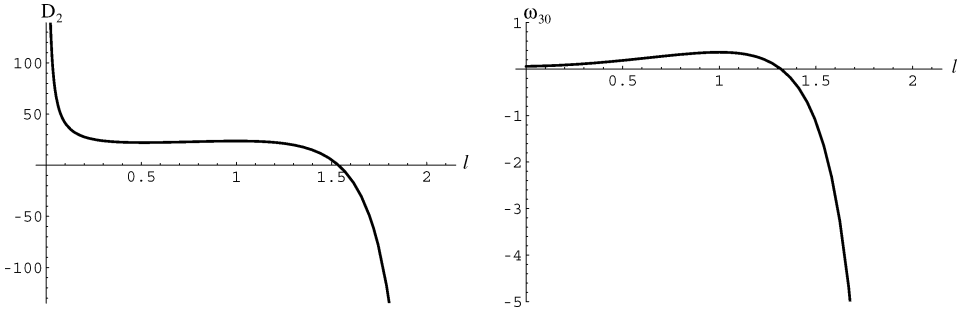

Fig. 3. The corrections D_2 and ω_{30} as functions of the boundary location $0 < \ell < 2.2$ when $L_1 = 2$.

We now suppose that the dynamo number is supercritical, $D = D_0 + \epsilon^2 D_2 + \epsilon^4 D_4 + \cdots + \delta$, where δ measures the distance from the threshold for the dynamo instability. We take $\delta = d\epsilon^2$, where $d = O(1)$. The growth rate $\sigma = \epsilon^2\delta\sigma_{21} + O(\epsilon^4\delta; \epsilon^2\delta^2; \delta^3)$ is positive:

$$\sigma_{21} = -\frac{2L_2(L_1-1)}{\omega_{10}(L_2-L_1)^2}, \tag{3.3}$$

and the corresponding frequency expansion takes the form $\omega = \epsilon\omega_{10} + \epsilon^3\omega_{30} + \epsilon\delta\omega_{11} + \epsilon^5\omega_{50} + \epsilon^3\delta\omega_{31} + O(\epsilon^7; \epsilon^5\delta; \epsilon^3\delta^2; \epsilon\delta^3)$.

We seek a solution of the nonlinear problem of the form

$$\begin{pmatrix} A \\ B \end{pmatrix} = \begin{pmatrix} A_0 \\ 0 \end{pmatrix} + \epsilon \begin{pmatrix} A_1 \\ B_1 \end{pmatrix} + \epsilon^2 \begin{pmatrix} A_2 \\ B_2 \end{pmatrix} + \cdots,$$

where A_0 is $O(1)$ but depends on x and t in the form $\epsilon(x+ct)$, as appropriate for a wave traveling towards the equator. A long computation, similar to that carried out in Ref. [7], now leads to a *reconstituted* amplitude equation

$$\frac{\partial C}{\partial \tau} - a\frac{\partial C}{\partial \xi} - a\frac{\partial^3 C}{\partial \xi^3} + bC^2\frac{\partial C}{\partial \xi} + \epsilon f = O\big(\epsilon^2\big) \tag{3.4}$$

for the quantity $C(\xi,\tau) = A_{0_\xi} + O(\epsilon)$, written in a reference frame traveling with the speed $c = \omega_{10} + \epsilon^2(\omega_{30} + d\omega_{11}) + \cdots$: $\xi = \epsilon(x+ct)$, $\tau \sim \epsilon^3 t$. Here

$$\begin{aligned} a &= \frac{2\omega_{10}^3}{45}\big[13 + 2L_1^4 + 15L_2^2 + 2L_2^4 \\ &\quad + 2L_1^3(7L_2 - 11) + 3L_1^2\big(21 - 20L_2 + 8L_2^2\big) \\ &\quad + 2L_1\big(-26 + 15L_2 - 15L_2^2 + 7L_2^3\big)\big], \\ b &= 3\omega_{10}^3(L_1 - L_2)^2 > 0, \end{aligned} \tag{3.5}$$

and

$$f = (\alpha a + \eta)\frac{\partial^2 C}{\partial \xi^2} + (\alpha a + \gamma)\frac{\partial^4 C}{\partial \xi^4} + (\beta - \alpha b)\frac{\partial^2}{\partial \xi^2}\left(\frac{1}{3}C^3\right), \tag{3.6}$$

where

$$\begin{aligned} \alpha &= -\frac{\omega_{10}}{6}\big[4\big(L_1^2 + L_2^2\big) + 7 + 2L_1(3L_2 - 7)\big], \\ \beta &= \frac{1}{2}\omega_{10}^4(L_1 - L_2)^2\big[1 + 2L_1(L_2 - 1)\big], \\ \gamma &= \frac{2D_2(1-L_1)L_2}{\omega_{10}(L_2-L_1)^2} - \alpha a, \\ \eta &= \gamma + \frac{2L_2(1-L_1)d}{\omega_{10}(L_2-L_1)^2}. \end{aligned} \tag{3.7}$$

When a and b are both $O(1)$ the leading order equation is the modified Korteweg–de Vries (mKdV) equation

$$\frac{\partial C_0}{\partial \tau} - a\frac{\partial C_0}{\partial \xi} - a\frac{\partial^3 C_0}{\partial \xi^3} + bC_0^2\frac{\partial C_0}{\partial \xi} = 0, \tag{3.8}$$

where $C = C_0 + O(\epsilon)$. The solutions of this equation depend on the relative signs of the coefficients a and b. The locations ℓ_a, say ($\ell_{\omega_1} < \ell_a < \ell_{\omega_2}$) at which the coefficient a changes sign, separate the situations in which traveling solutions $C_0(\xi,\tau) \equiv C_0(\Xi)$, $\Xi \equiv \xi - v\tau$, take the form of snoidal waves and kinks, from those in which cnoidal and solitary waves are found (see below). Fig. 4 shows that for $L_1 = 2$ there is only one such position, $\ell_a \approx 1.7$. When $a > 0$ and $a + v > 0$ snoidal wave solutions of the form

$$C_0 = N_{\rm sn}\,\mathrm{sn}(\mu_{\rm sn}\Xi, s), \tag{3.9}$$

where

$$\begin{aligned} N_{\rm sn}^2 &= \frac{6(a+v_{\rm sn})}{b}\left(\frac{s^2}{1+s^2}\right), \\ \mu_{\rm sn}^2 &= \left(1 + \frac{v_{\rm sn}}{a}\right)\frac{1}{1+s^2}, \end{aligned} \tag{3.10}$$

are present. Here sn, and cn below, are the usual elliptic functions and $0 \leqslant s < 1$ is their modulus. Both have period $4K(s)/\mu$, where $K(s)$ is the complete elliptic integral of the first kind. As $s \to 1^-$, the snoidal waves degenerate into kinks,

$$C_0 = N_k \tanh(\mu_k \Xi), \tag{3.11}$$

where

$$N_k^2 = \frac{3(a+v_k)}{b}, \qquad \mu_k^2 = \frac{1}{2}\left(1 + \frac{v_k}{a}\right). \tag{3.12}$$

For $a < 0$ the solutions take the form of cnoidal waves

$$C_0 = N_{\rm cn}\,\mathrm{cn}(\mu_{\rm cn}\Xi, s), \tag{3.13}$$

where

$$\begin{aligned} N_{\rm cn}^2 &= \frac{6(a+v_{\rm cn})}{b}\left(\frac{s^2}{2s^2-1}\right), \\ \mu_{\rm cn}^2 &= \left(1 + \frac{v_{\rm cn}}{a}\right)\frac{1}{1-2s^2}, \end{aligned} \tag{3.14}$$

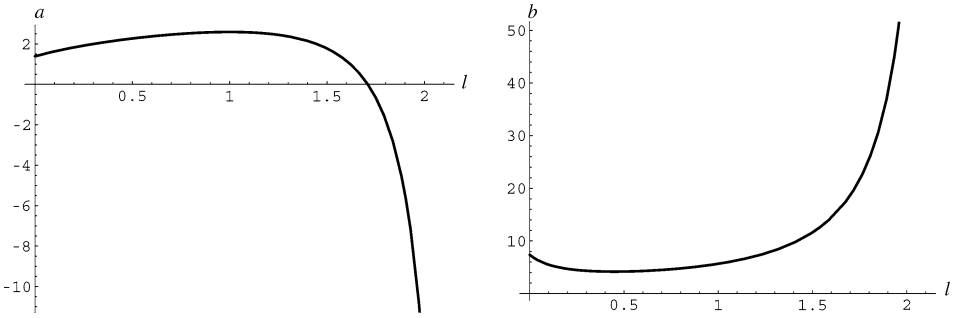

Fig. 4. The coefficients a and b in the mKdV equation (3.8) as functions of the boundary location $0 < \ell < 2.2$ when $L_1 = 2$ ($\ell_a \approx 1.7$).

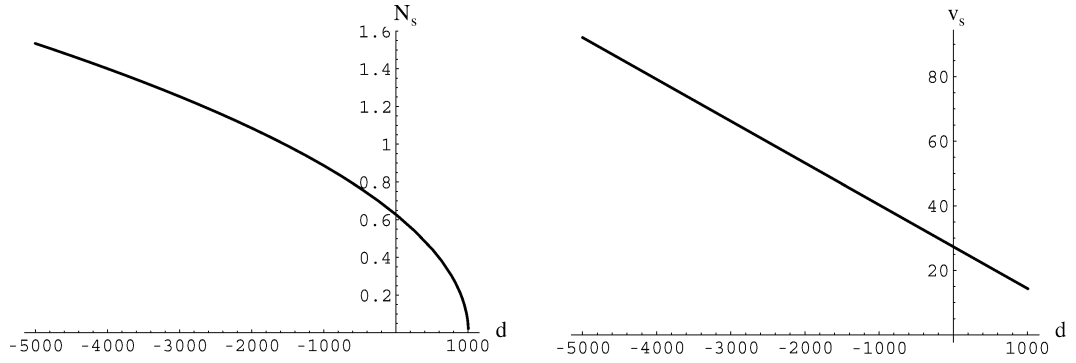

Fig. 5. The soliton amplitude N_s (left) and the speed v_s (right) as functions of d. Note that $N_s \to 0$ as $d \to -D_2 > 0$ ($L_1 = 2$, $\ell = 2$).

provided that $s^2 > 1/2\,(a + v_{\rm cn} > 0)$, and $s^2 < 1/2\,(a + v_{\rm cn} < 0)$. The former degenerate into *solitary* waves,

$$C_0 = N_s \operatorname{sech}\left[\left(-\frac{N_s^2 b}{6a}\right)^{1/2} \Xi\right], \quad N_s^2 = \frac{6(a+v_s)}{b}, \tag{3.15}$$

as $s \to 1^-$.

In addition, when $a < 0$ localized time-dependent states known as *breathers* are present. These take the form

$$C_0(\Theta, t) = -2\sqrt{\frac{6(-a)^{1/3}}{b}} \times \frac{\partial}{\partial \Theta}\left\{\arctan\left(\frac{\lambda \sin(\kappa\Theta + \zeta t + \phi)}{\kappa \cosh(\lambda\Theta + \eta t + \psi)}\right)\right\}, \tag{3.16}$$

where $\Theta = (-a)^{-1/3}(\xi + a\tau)$, $\zeta = \kappa(\kappa^2 - 3\lambda^2)$, $\eta = \lambda(3\kappa^2 - \lambda^2)$ and ϕ, ψ are arbitrary constants.

4. The perturbed mKdV equation

When $D_2 \sim O(1)$ the amplitude of these waves evolves on the timescale ϵ^{-4}, as described by the *perturbed* mKdV equation (3.4). For the soliton (3.15) the perturbation selects the amplitude N_s, given by the equation (cf. [1,3,10–12])

$$\frac{\partial N_s}{\partial t} = \hat{f} + O(\epsilon), \tag{4.1}$$

where

$$\hat{f} = -\frac{bN_s^3}{6a}\left(\frac{2}{3}(\alpha a + \eta) + \frac{N_s^2}{15}\left[4(\beta - \alpha b) + \frac{7b}{3a}(\alpha a + \gamma)\right]\right).$$

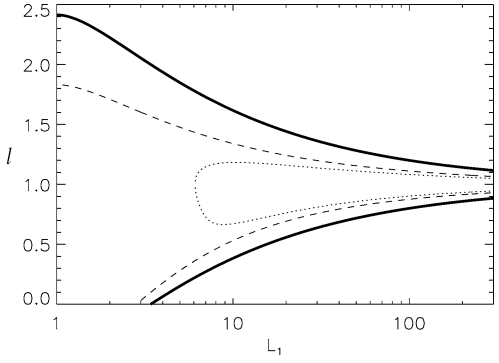

Fig. 6. The existence and stability of solitary waves in the (L_1, ℓ) plane. The frequency ω_{10} is real between the solid curves (and the abscissa and ordinate); solitary waves lie inside this region but outside the dashed lines along which $a = 0$. The stability region for such waves (the interior of the dotted curve where $\hat{h} > 0$) is disjoint, indicating that solitary waves are unstable.

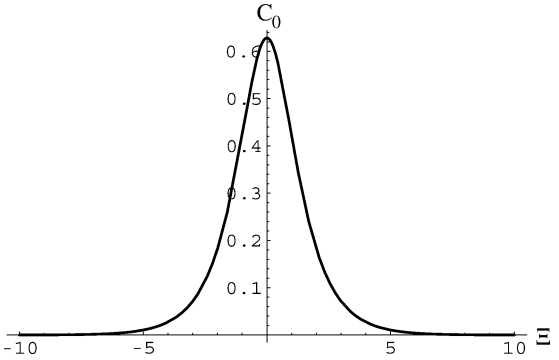

Fig. 7. The solitary wave C_0 as a function of $\Xi \equiv \xi - v_s\tau$ for $d = 1$ ($L_1 = 2$, $\ell = 2$).

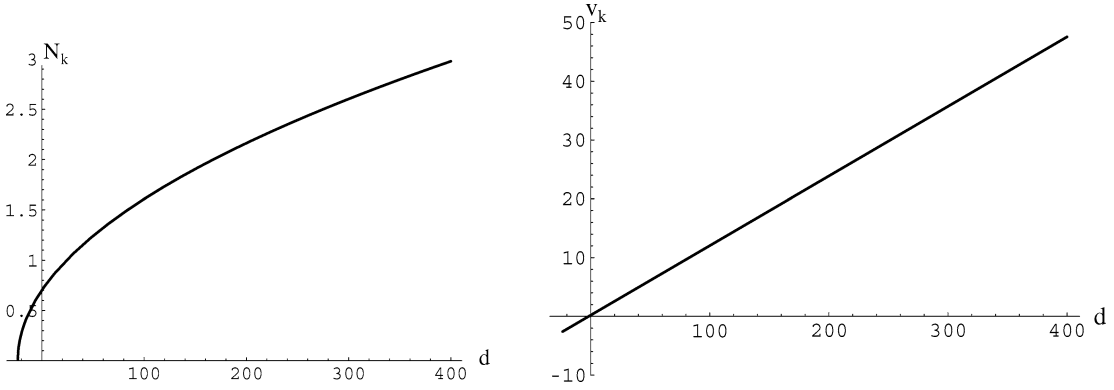

Fig. 8. The kink amplitude N_k (left) and speed v_k (right) as functions of d ($L_1 = 2$, $\ell = 1$).

Thus

$$N_s^2 \equiv 30aL_2(L_1 - 1)(D_2 + d)/b\hat{h}, \tag{4.2}$$

where $\hat{h} \equiv 7D_2(1 - L_1)L_2 - 12a(L_2 - L_1)^2$. The resulting bifurcation diagram $N_s(d)$ and the corresponding speed $v_s(d)$ are shown in Fig. 5 for $L_1 = \ell = 2$. Since $v_s > 0$ the solitary waves travel towards the equator more slowly than infinitesimal waves. The (amplitude) stability of the waves is given by

$$\left.\frac{\partial \hat{f}}{\partial N_s}\right|_{N_s} = -\frac{2b^2 N_s^4 \hat{h}}{135a^2\omega_{10}(L_2 - L_1)^2}.$$

Since $a < 0$ it follows that solitary waves exist and are stable if $D_2 + d > 0$ and $\hat{h} > 0$. However, Fig. 6 shows that these conditions are mutually exclusive, i.e., that when $a < 0$ $\hat{h}$ is also negative. Thus all solitary waves are unstable, as suggested by the bifurcation diagram in Fig. 5. The solitary wave present at $d = 1$ ($L_1 = \ell = 2$) is shown in Fig. 7.

For the kink (3.11) the effect of the perturbation is to select the amplitude N_k given by

$$N_k^2 \equiv 15aL_2(1 - L_1)(D_2 + d)/b\bar{h}, \tag{4.3}$$

where $\bar{h} \equiv 2D_2(1 - L_1)L_2 + 3a(L_2 - L_1)^2$. The corresponding bifurcation diagram $N_k(d)$ and the speed $v_k(d)$ are shown in Fig. 8. Note that kinks can travel faster ($v_k < 0$) or slower ($v_k > 0$) than infinitesimal waves depending upon the value of d. The stability (and existence) again depends on the sign of D_2 and $\bar{h}$. One finds that kinks exist and are stable when $a > 0$ and $D_2 > 0$, while if $D_2 < 0$ and $\bar{h} > 0$ the kinks exist and are stable only for $d > |D_2|$. In contrast, if $D_2 < 0$ and $\bar{h} < 0$ kinks exist only for $d < |D_2|$, but are then unstable. In particular, when $d = 1$ ($L_1 = 2$, $\ell = 1$) the kink state (Fig. 9) is stable.

The solitary waves and kinks found above *coexist* with cnoidal and snoidal waves of different spatial periods, i.e., with extended wavetrains. For these the perturbation ϵf produces a slow drift in the modulus s [7]; the fixed point of this drift determines the modulus $\bar{s}$ say, and hence the amplitude and speed of the waves as a function of the distance from the threshold for the dynamo instability. The resulting bifurcation diagram $N_{\rm sn}(d)$ and speed $v_{\rm sn}(d)$ for snoidal waves of spatial period 2π, obtained by eliminating $v_{\rm sn}$ from Eq. (3.10), are shown in Fig. 10 (for $L_1 = 2$, $\ell = 1$). Both solutions are compared with weakly nonlinear results [7], shown as dashed lines. Since the primary

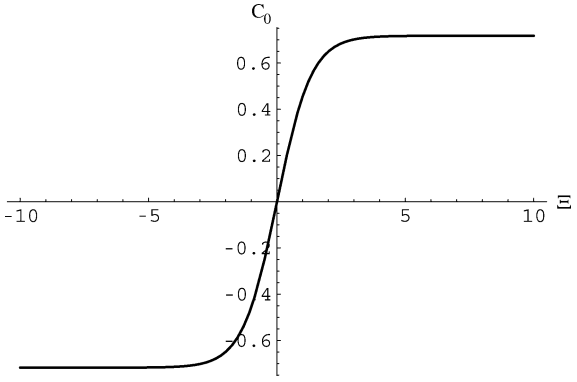

Fig. 9. The kink C_0 as a function of $\Xi \equiv \xi - v_k\tau$ for $d = 1$ ($L_1 = 2$, $\ell = 1$).

bifurcation is *supercritical* the snoidal waves are stable with respect to 2π-periodic perturbations. The corresponding results for 2π-periodic cnoidal waves are shown in Fig. 11. These also bifurcate supercritically and hence are initially stable with respect to 2π-periodic perturbations. However, at larger d the stable cnoidal waves are annihilated at a saddle-node bifurcation by unstable cnoidal waves; thus 2π-periodic cnoidal waves exist over a limited range of d only.

4.1. Physical manifestation of the solution

The solutions for the fields A_0, A_1 and B_1 can be reconstructed for each type of wave. For the solitary wave (3.15) we obtain

$$A_0 = N_s\left(-\frac{24a}{bN_s^2}\right)^{1/2} \arctan\left[\tanh\left(\left(-\frac{N_s^2 b}{24a}\right)^{1/2}\Xi\right)\right],$$

for the kink (3.11)

$$A_0 = \frac{N_k}{\mu_k} \ln\left|\cosh\left(\left(\frac{N_k^2 b}{6a}\right)^{1/2}\Xi\right)\right|,$$

for the snoidal wave (3.9)

$$A_0 = \frac{N_{\rm sn}}{s\mu_{\rm sn}} \ln\bigl[\mathrm{dn}(\mu_{\rm sn}\Xi, s) - s\,\mathrm{cn}(\mu_{\rm sn}\Xi, s)\bigr],$$

and for the cnoidal wave (3.13)

$$A_0 = \frac{N_{\rm cn}}{s\mu_{\rm cn}} \arccos\bigl[\mathrm{dn}(\mu_{\rm cn}\Xi, s)\bigr],$$

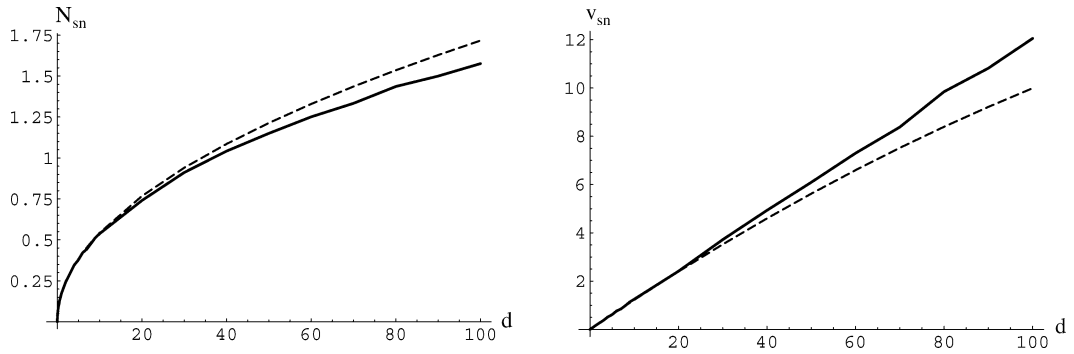

Fig. 10. The amplitude $N_{\rm sn}$ (left) and speed $v_{\rm sn}$ (right) as functions of d for 2π-periodic snoidal waves (solid line) together with the corresponding result obtained from second order perturbation theory (dashed line) ($L_1 = 2$, $\ell = 1$).

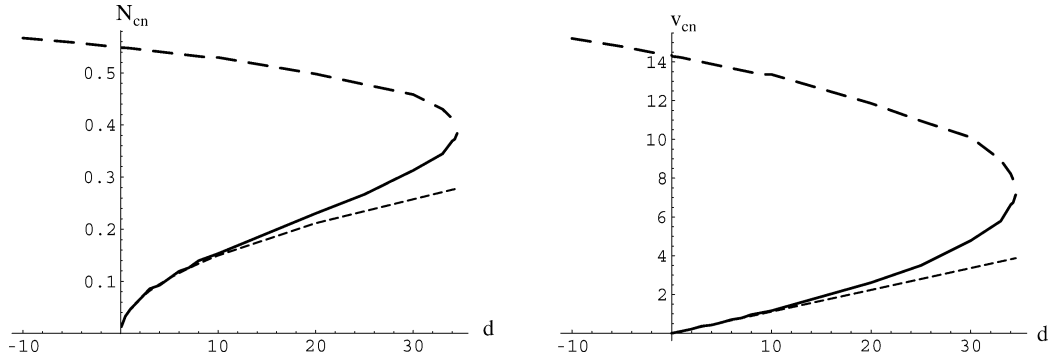

Fig. 11. The amplitude $N_{\rm cn}$ (left) and speed $v_{\rm cn}$ (right) as functions of d for 2π-periodic cnoidal waves (solid line—stable branch; long dashed line—unstable branch) together with the corresponding result obtained from second order perturbation theory (short dashed line). The unstable branch may be traced backwards into $d < 0$, and for $d \approx -5000$ the fixed point $\bar{s} \approx 1$ ($L_1 = 2$, $\ell = 2$).

to within an arbitrary phase. In each case

$$A_1 = N\omega_{10}\left(\frac{1}{2}z^2 - L_1 z + L_1 - L_2\right)\rho(\Xi) + b_5 \quad \text{in } z > 1,$$

$$A_1 = N\omega_{10}\left(\frac{1}{2}z^2 - L_2 z\right)\rho(\Xi) + b_5 \quad \text{in } z < 1,$$

$$B_1 = \frac{NL_2D_0(L_1 - z)}{L_2 - L_1}\rho(\Xi) \quad \text{in } z > 0,$$

$$B_1 = \frac{NL_1D_0(L_2 - z)}{L_2 - L_1}\rho(\Xi) \quad \text{in } z < 0,$$

where $\rho = \rho_s$, ρ_k, $\rho_{\rm sn}$, $\rho_{\rm cn}$, respectively, and

$$\rho_s(\Xi) = \operatorname{sech}\left[\left(-\frac{N_s^2 b}{6a}\right)^{1/2}\Xi\right],$$

$$\rho_k(\Xi) = \tanh\left[\left(\frac{N_k^2 b}{6a}\right)^{1/2}\Xi\right],$$

$$\rho_{\rm sn}(\Xi, s) = \operatorname{sn}(\mu_{\rm sn}\Xi, s), \qquad \rho_{\rm cn}(\Xi, s) = \operatorname{cn}(\mu_{\rm cn}\Xi, s).$$

Fig. 12 shows the vertical profiles of $B_1(\Xi, z)$ at Ξ chosen to correspond to a maximum of $C_0 \equiv A_{0_\xi}$ in each case. The leading order contributions to both the toroidal and poloidal fields are shown together in Fig. 13; both are of order ϵ, despite the fact that $A_0 = O(1)$.

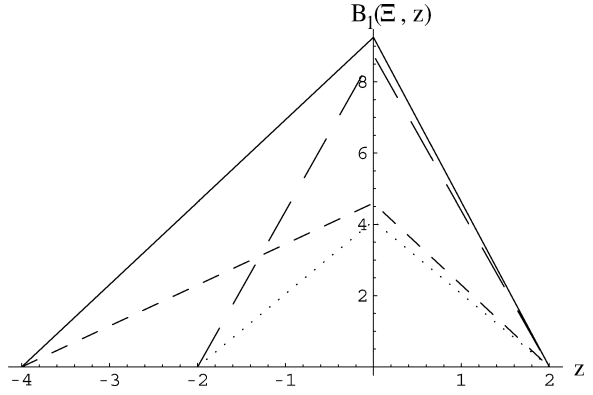

Fig. 12. Profiles of $B_1(\Xi, z)$ for each type of wave at Ξ corresponding to maxima of C_0: (a) An unstable solitary wave (solid line, $\Xi = 0$, $d = 1$, $L_1 = 2$, $\ell = 2$). (b) A kink (dotted line, $\Xi = 10$, $d = 1$, $L_1 = 2$, $\ell = 1$; $B_1(0, z) = 0$, $B_1(-10, z) = -B_1(10, z)$). (c) A snoidal wave (long dashed line, $\Xi = \pi/2$, $d = 100$, $\bar{s} \approx 0.96$, $L_1 = 2, \ell = 1$; $B_1(3\pi/2, z) = -B_1(\pi/2, z)$). (d) A stable cnoidal wave (short dashed line, $\Xi = 0$, $d = 30$, $\bar{s} \approx 0.45$, $L_1 = 2$, $\ell = 2$; $B_1(\pi, z) = -B_1(0, z)$).

5. Discussion

In this Letter we have shown that mean-field dynamo equations with α-quenching possess solitary wave solutions. These satisfy at leading order the modified KdV equation; corrections to this equation incorporate both forcing and dissipation, and permit us to identify the amplitude and velocity of the solitary wave as a function of the distance from the threshold for the dy-

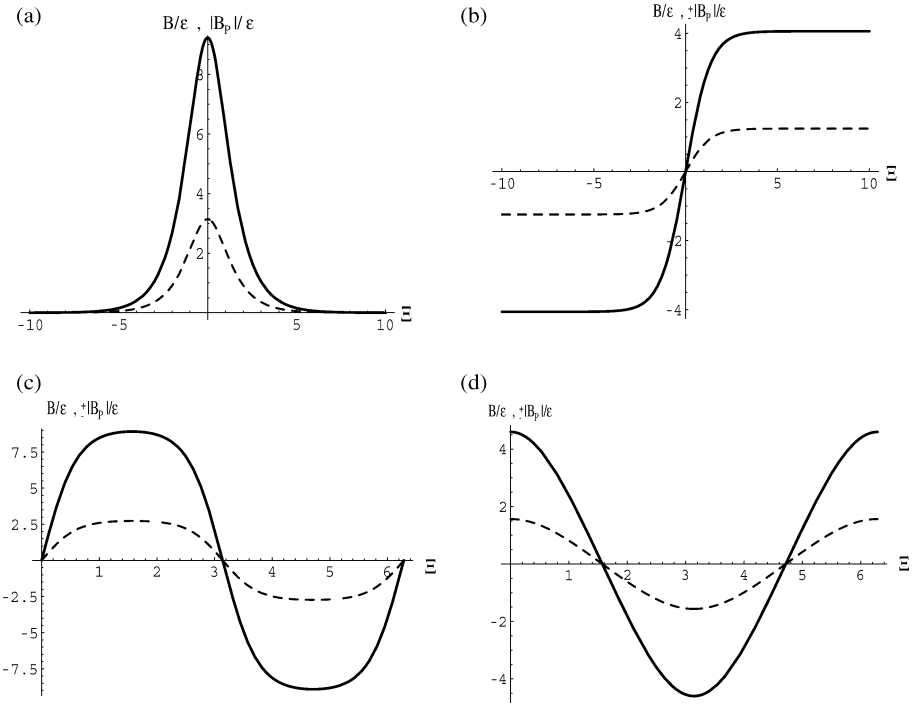

Fig. 13. The toroidal field (B/ϵ, solid line) and poloidal field ($|B_P|/\epsilon$, $|B_P|^2 \equiv \epsilon^2[(\partial A_1/\partial z)^2 + (\partial A_0/\partial \xi)^2]$, dashed line) at $z = 0$. (a) An unstable solitary wave ($d = 1$, $L_1 = 2$, $\ell = 2$). (b) A kink ($-|B_P|/\epsilon$ for $\Xi \leqslant 0$ and $|B_P|/\epsilon$ for $\Xi \geqslant 0$, $d = 1$, $L_1 = 2$, $\ell = 1$). (c) A snoidal wave ($|B_P|/\epsilon$ for $\Xi \leqslant \pi$ and $-|B_P|/\epsilon$ for $\Xi \geqslant \pi$, $d = 100$, $\bar{s} \approx 0.96$, $L_1 = 2$, $\ell = 1$). (d) A stable cnoidal wave ($-|B_P|/\epsilon$ for $\pi/2 \leqslant \Xi \leqslant 3\pi/2$ and $|B_P|/\epsilon$ otherwise, $d = 30$, $\bar{s} \approx 0.45$, $L_1 = 2$, $\ell = 2$).

namo instability. The solitary wave moves with an $O(1)$ speed towards the equator. Since the modified KdV equation is completely integrable the leading order solitary waves are in fact solitons, and will interact like solitons do. The extent to which such soliton-like interactions persist in the presence of the perturbation ϵf remains to be elucidated. However, it is evident that the 'butterfly' diagram used to represent the solar dynamo will be substantially modified. We have also shown that these solitary waves coexist with a one-parameter family of nonlinear wavetrains, but were not successful in elucidating the relative stability among solutions with different wavelengths.

Solitary waves are possible when the coefficient a in Eq. (3.8) is negative. In the transition region $\ell \sim \ell_a$ the problem is described by two different equations, depending on how close ℓ is to ℓ_a. When $a = \epsilon^q a_0$, $0 < q < 1$, $a_0 = O(1)$, we have the equation

$$\frac{\partial C}{\partial \tau} + C^2 \frac{\partial C}{\partial \zeta} - \epsilon^q \operatorname{sgn}(a_0) \frac{\partial^3 C}{\partial \zeta^3} = 0, \tag{5.1}$$

where $\zeta = \xi + \epsilon^q a_0 \tau$, and both $b_* \equiv b(\ell_a) > 0$ and a_0 have been absorbed into a rescaling of C and ζ. The resulting problem is similar to the zero-dispersion limit of the KdV equation [5] except that here the equation in question is the mKdV. In contrast, when a_0 is smaller, viz., $a = \epsilon a_0$, $a_0 = O(1)$, the system is described by a perturbed Burgers-like equation

$$\frac{\partial C}{\partial \tau} + b_* C^2 \frac{\partial C}{\partial \xi} + \epsilon \left[\eta_* \frac{\partial^2 C}{\partial \xi^2} + \gamma_* \frac{\partial^4 C}{\partial \xi^4} + (\beta_* - \alpha_* b_*) \frac{\partial^2}{\partial \xi^2} \left(\frac{1}{3} C^3 \right) - a_0 \frac{\partial C}{\partial \xi} - a_0 \frac{\partial^3 C}{\partial \xi^3} \right] = O(\epsilon^2), \tag{5.2}$$

where the subscript $*$ again indicates that quantities are evaluated at $\ell = \ell_a$. It follows that, in a frame moving southwards with speed near ϵa_0, solutions with $O(\epsilon^{-1})$ wavelength evolve on the slower time scale $T = \epsilon \tau$ according to

$$\frac{\partial C}{\partial T} + C^2 \frac{\partial C}{\partial \zeta} + \epsilon^2 \left[\eta_* \frac{\partial^2 C}{\partial \zeta^2} + \left(\frac{\beta_*}{b_*} - \alpha_* \right) \frac{\partial^2}{\partial \zeta^2} \left(\frac{1}{3} C^3 \right) \right] = O(\epsilon^3), \tag{5.3}$$

where

$$\frac{\beta_*}{b_*} - \alpha_* = -\frac{2}{\omega_{10_*}} < 0,$$

$$\eta_* = \left. \frac{2L_2(1 - L_1)(D_2 + d)}{\omega_{10}(L_2 - L_1)^2} \right|_{\ell = \ell_a}.$$

In writing Eq. (5.3) we have absorbed a coefficient $b_* + O(\epsilon)$ into a rescaling of C. The resulting equation is again a Burgers-like equation but this time with (nonlinear) viscous regularisation. Eq. (5.2) thus describes the cross-over between dispersive and viscous regularisation of the shocks that form when $\epsilon = 0$. Of particular interest is the possibility that $\eta_* > 0$, indicating that infinitesimal perturbations produce immediately a sea of shocks that provide stochastic forcing for the nonlinear problem [2].

The above remarks indicate that as ℓ increases the dynamo waves within the model can change from snoidal waves or kinks to cnoidal or solitary waves (and vice versa), and that this transition involves the formation of shock-like structures. These

possibilities raise significant mathematical questions in their own right.

Acknowledgements

This work was supported by the National Science Foundation under grant DMS-0305968 and by the High Altitude Observatory. We thank B. Birnir for a stimulating discussion of Eq. (5.3) with $\eta_* > 0$ and T.J. Bogdan for helpful comments.

References

[1] H. Aspe, M.C. Depassier, Phys. Rev. A 41 (1990) 3125.
[2] B. Birnir, T.R. Smith, G.E. Merchant, Comput. Geosci. 27 (2001) 1189.
[3] T. Kawahara, Phys. Rev. Lett. 51 (1983) 381.
[4] N.I. Kleeorin, A.A. Ruzmaikin, Geophys. Astrophys. Fluid Dyn. 17 (1981) 281.
[5] P.D. Lax, C.D. Levermore, Commun. Pure Appl. Math. 36 (1983) 253.
[6] J. Mason, D.W. Hughes, S.M. Tobias, Astrophys. J. 580 (2002) L89.
[7] J. Mason, E. Knobloch, Physica D 205 (2005) 100.
[8] H.K. Moffatt, Magnetic Field Generation in Electrically Conducting Fluids, Cambridge Univ. Press, Cambridge, 1978.
[9] M. Ossendrijver, Astron. Astrophys. Rev. 11 (2003) 287.
[10] E. Ott, R.N. Sudan, Phys. Fluids 12 (1969) 2388.
[11] E. Ott, R.N. Sudan, Phys. Fluids 13 (1970) 1432.
[12] E. Ott, W.M. Manheimer, D.L. Book, J.P. Boris, Phys. Fluids 16 (1973) 855.
[13] A.A. Ruzmaikin, A.M. Shukurov, D.D. Sokoloff, Magnetic Fields of Galaxies, Kluwer Academic, Dordrecht, 1988.
[14] J. Schou, et al., Astrophys. J. 505 (1998) 390.
[15] M. Steenbeck, F. Krause, K.H. Rädler, Z. Naturforsch. A 21 (1966) 369.
[16] N.O. Weiss, in: M.R.E. Proctor, A.D. Gilbert (Eds.), Lectures on Solar and Planetary Dynamos, Cambridge Univ. Press, Cambridge, 1994, pp. 59–95.